ISSN 0021-3640, JETP Letters, 2023, Vol. 117, No. 8, pp. 557–565. © The Author(s), 2023. This article is an open access publication.
Russian Text © The Author(s), 2023, published in Pis'ma v Zhurnal Eksperimental'noi i Teoreticheskoi Fiziki, 2023, Vol. 117, No. 8, pp. 561–570.

FIELDS, PARTICLES, AND NUCLEI

# Measurement of the Cross Section for the Neutron-Induced Fission of $^{238}$U Nuclei in the Energy Range of 0.3–500 MeV

**A. S. Vorobyev[a, *] (ORCID: 0000-0002-9607-958X), A. M. Gagarski[a] (ORCID: 0000-0003-4880-4115), O. A. Shcherbakov[a] (ORCID: 0000-0001-6278-4005), L. A. Vaishnene[a] (ORCID: 0000-0002-7422-0749), and A. L. Barabanov[b, c] (ORCID: 0000-0003-4573-6591)**

[a] *Petersburg Nuclear Physics Institute, National Research Center Kurchatov Institute, Gatchina, 188300 Russia*
[b] *National Research Center Kurchatov Institute, Moscow, 123182 Russia*
[c] *National Research Nuclear University MEPhI (Moscow Engineering Physics Institute), Moscow, 115409 Russia*
**e-mail: vorobyev_as@pnpi.nrcki.ru*

Received March 14, 2023; revised March 14, 2023; accepted March 18, 2023

The cross section for the neutron-induced fission of $^{238}$U nuclei has been measured using the time-of-flight spectrometer of the GNEIS neutron complex at the Petersburg Nuclear Physics Institute, National Research Center Kurchatov Institute, in the neutron energy range of 0.3–500 MeV. Fission fragments have been detected by low-pressure position-sensitive multiwire proportional counters. The cross section for $^{238}$U($n$, $f$) fission has been measured with respect to the cross section for $^{235}$U($n$, $f$) fission, which is an accepted international standard. Data on the energy dependence of the anisotropy of the angular distribution of fragments of neutron-induced $^{238}$U nuclei are also presented. The data obtained have been compared to previous experiments carried out using both similar and significantly different methods.

**DOI:** 10.1134/S0021364023600787

It is currently believed that the nuclear power industry will be developed in the way to the implementation of a closed fuel cycle including fourth-generation nuclear power installations [1, 2] and nuclear reactors driven by high-current proton accelerators with energies of 1 GeV and above (accelerator driven systems) [3]. These systems will ensure the safety and reliability of the nuclear power industry, its economic competitiveness owing to a lower life-cycle cost compared to other power sources, and more efficient use of nuclear fuel with the simultaneous reduction of the yield of nuclear waste. The solution to problems of accumulation, storage, and possible utilization of spent nuclear fuel is relevant. According to data for 2020, the worldwide amount of spent nuclear fuel is 400000 t including 275000 t stored in repositories, where 7000 t are added annually [4]. The transmutation of nuclear waste in fast reactors currently seems one of the promising methods to reduce the radiotoxicity of spent nuclear fuel. However, practical fabrication of novel nuclear installations and utilization of radioactive waste are impossible without reliable and accurate nuclear data.

The cross sections for the fission of the main $^{235}$U and $^{238}$U isotopes induced by neutrons with energies up to 200 MeV are currently accepted as standards [5, 6]; for this reason, particular attention is paid to their measurement. These measurements cover both the range of 1–20 MeV (reactor spectrum), which is used in current and near future nuclear technologies, and the range of 20 MeV to 1 GeV and above, which is most experimentally difficult but is decisively important for the development of promising accelerator driven technologies. The results of experiments on the measurement of the cross section of neutron-induced fission of $^{238}$U nuclei can be found in the EXFOR experimental nuclear reaction database [7].

Data on the cross section for the neutron-induced fission of $^{238}$U nuclei exist generally for neutron energies below 20 MeV, which are interesting for calculations of nuclear reactors. Most of these data were obtained with monoenergetic neutrons from various reactions at accelerators [8–17]. The main feature of such measurements is that an individual experiment was carried out for each energy (or a chosen energy range) of neutrons inducing fission. Different reactions and neutron-emitting targets were used and additional adjustment (calibration) of all detecting instruments was sometimes performed. To test data on the fission cross sections of $^{238}$U nuclei measured with monoenergetic neutron beams and to estimate their accuracy, similar experiments were also carried out with neutron beams with a continuous spectrum using the time-of-flight method [18, 19]. Measurements at neutron energies above 20 MeV were performed both with quasimonoenergetic neutron beams [20, 21] and

with neutron beams with the continuous spectrum using the time-of-flight method [22–27]. The first results were also obtained recently at the China Spallation Neutron Source [28, 29]. A gas scintillation counter [8], thin-film breakdown counters [20], a time projection chamber [27], and fission ionization chambers [9–19, 21–24, 28, 29] were used in the cited works to detect fission fragments. Measurements in [25, 26] were carried out with a multisection ionization chamber and an array of position-sensitive parallel plate avalanche counters in various geometries.

In all works cited above, except for [15], where direct measurements were performed, the fission cross section of the nucleus under study was measured with respect to the cross section of a reaction that is known with a high accuracy (standard cross section) such as $^{1}H(n,n)p$ ($n$–$p$ scattering) [17, 20, 21], $^{27}Al(n,\alpha)^{24}Na$ and $^{56}Fe(n,p)^{56}Mn$ reactions [16], and the neutron-induced fission of $^{235}U$ nuclei [8–14, 18, 19, 22–29]. This procedure allowed one to minimize errors caused by the uncertainty of the neutron flux. In addition to the relative method of measurements of the fission cross section, the mixed target method [9–11, 13, 14, 18, 19, 23] is often used for nuclei whose fission cross section has a threshold; this method also makes it possible to minimize the error caused by the uncertainty of the mass of studied samples.

The comparison of existing experimental data reveals some spread at neutron energies above 30 MeV. In particular, the authors of [22, 24, 25, 29] believe that their data are in general agreement with each other, whereas the data reported in [23] are systematically lower and the maximum relative difference of ~8% is observed for neutron energies above 100 MeV. The data from [20, 21] have a higher uncertainty than the data cited above, they are ~7% higher than the data from [22, 24, 25, 29] at energies below 100 MeV, and the data from [21] at neutron energies above 100 MeV are in agreement with the data both from [23] and from [22, 24, 25, 29].

In this work, the fission cross section of $^{238}U$ nuclei is measured at the GNEIS neutron complex [30, 31] (Petersburg Nuclear Physics Institute, National Research Center Kurchatov Institute) based on the SC-1000 synchrocyclotron with a 1-GeV proton beam. The GNEIS neutron complex includes an intense pulsed neutron source (~$10^{14}$ neutrons per second in a solid angle of $4\pi$) with a pulse duration of ~10 ns and a repetition frequency of ~50 Hz and a time-of-flight spectrometer having five neutron beams with bases up to 50 m. A fast neutron pulse is formed by the incidence of the proton beam on a 400 × 100 × 50-mm water-cooled lead target placed in the vacuum chamber of the accelerator. It is noteworthy that the time between successive incidences of the proton beam on the lead target is ~20 ms, which corresponds to the energy of recycling neutrons less than 0.017 eV at a time-of-flight base of (36.5 ± 0.05) m used in these measurements. To exclude such recycling neutrons, we used a 0.1-mm-thick Cd filter (in this case, the transmission of neutrons with energies below 0.3 eV can be neglected), which was placed in the hall of the SC-1000 synchrocyclotron behind a 6-m-thick hard concrete wall at a distance of 14 m from the measuring instruments. The cross section for the $^{238}U(n,f)$ fission with respect to the cross section for the $^{235}U(n,f)$ fission was measured on neutron beam no. 5 with a diameter of 90 mm.

Targets with the studied $^{238}U$ and $^{235}U$ nuclei were fabricated at the Khlopin Radium Institute (St. Petersburg) by the "painting" method on aluminum substrates 0.1 mm in thickness. The shapes and sizes of the active layer were different. The circular 99.996%-enriched $^{238}U$ target had a thickness of (1150 ± 56) μg/cm$^2$ and a diameter of 60 mm, and the 100 × 50-mm rectangular 99.992%-enriched $^{235}U$ target had a thickness of (203 ± 11) μg/cm$^2$. The homogeneity of the active layer determined by scanning the α activity of the target by silicon detectors with a small solid angle was 10%.

To ensure identical conditions for measurements of fission cross sections, a 0.1-mm-thick aluminum screen was placed on the active layer of the $^{238}U$ and $^{235}U$ targets and was used to separate a circular region with a diameter of (48.0 ± 0.1) mm on the surface of the active layer. Further, the total α activity of the $^{238}U$ and $^{235}U$ targets with the deposited screen, which did not transmit α particles and fission fragments, was measured using silicon detectors at the Petersburg Nuclear Physics Institute, National Research Center Kurchatov Institute. The masses of the $^{238}U$ and $^{235}U$ isotopes in the targets used to measure fission cross sections were determined from the measured activity with a statistical accuracy of 0.6 and 0.9%, respectively. The measured ratio $N_{U8}/N_{U5}$ of the number of the main isotope nuclei in the $^{238}U$ and $^{235}U$ targets was 5.364 ± 0.083, which coincides within measurement errors with the estimate obtained at the Khlopin Radium Institute.

The sketch of the experimental setup and the data acquisition and preliminary processing system is presented in Fig. 1. The experimental setup for measuring the fission cross sections consists of the array of two low-pressure position-sensitive multiwire proportional counters (MWPCs) [32], a fission ionization chamber with $^{238}U$ targets for the relative monitoring the neutron flux, and a photomultiplier tube placed in the neutron beam to form a start signal of a neutron pulse (start detector). This setup is a modified version of the setup previously used to measure the angular distributions of fission fragments [33–37].

Fission fragments emitted from the target with the studied $^{238}U$ isotope and from the target with the reference $^{235}U$ isotope were detected in the same measuring run by the array of two MWPCs, which were

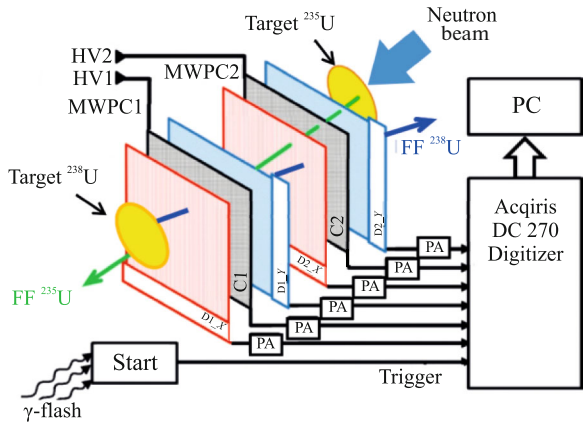


**Fig. 1.** (Color online) Sketch of the experimental setup and data acquisition system: (Start) start detector; (PA) preamplifier; (HV1, HV2) high-voltage sources; (D1 X, D2 X) anodes of detectors 1 and 2 (*X* axis), respectively; (D1 Y, D2 Y) anodes of detectors 1 and 2 (*Y* axis), respectively; and (C1, C2) cathodes of multiwire proportional counters 1 and 2, respectively.

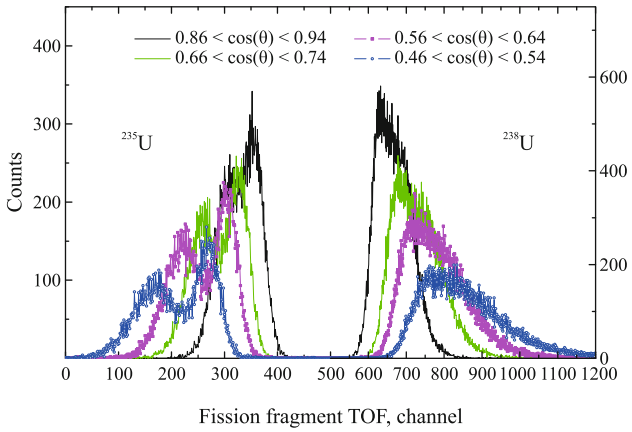


**Fig. 2.** (Color online) Time-of-flight spectrum of fission fragments of (left part) $^{235}$U and (right part) $^{238}$U nuclei from the 480th channel at various angles θ.

placed in the center of a cylindrical chamber with diameter of 28 cm and with thickness of walls of 2 mm filled with isobutane at a pressure of 8 mbar. The chamber on the neutron beam was oriented in such a way that the axis of the beam coincided with the axis of the chamber and was perpendicular to the planes of the targets and the electrodes of the MWPCs. Circular 0.5-mm-thick steel input and output windows 14 cm in diameter were made in the bases of the cylindrical chamber where the neutron beam passed. The distances from the targets with the studied and reference nuclei to the cathode of the first (second) MWPC were 6 and 37 mm (37 and 6 mm), respectively.

Each of the two MWPCs consisted of three wire electrodes including two anodes and one cathode. Signals from the two anodes and the cathode of each MWPC, as well as a signal from the monitor fission ionization chamber with $^{238}$U targets, were fed through fast preamplifiers to seven inputs of two 8-bit 500-MHz Acqiris DC270 digitizers, and a signal from the start detector was fed to the eighth input of the digitizers. At each incidence of the proton pulse on the lead target of the spectrometer of the GNEIS neutron complex, the digitizers were triggered by signals from the start detector, which recorded γ-ray photons and neutrons emitted from this target. The total signal digitizing time in all eight input of a digitizer was 8 μs, which corresponds to neutron energies from ~0.1 MeV to 1 GeV. Then, the waveforms obtained from waveform digitizers were read to a computer, where they were stored on a hard disk for the online control of received information and subsequent offline processing. Angular distributions of fission fragments were obtained by analyzing the resulting waveforms, and the ratio of the fission cross sections of the studied and reference nuclei was determined.

Since the neutron inducing fission transfers the momentum to the fissioning nucleus, the measured angular distribution of fission fragments differs from the angular distribution in the center-of-mass system of the fissioning nucleus. To take into account this effect, the fission cross sections and angular distributions of fission fragments were measured for two orientations of the setup with respect to the incident neutron beam, where the longitudinal component of the momentum of a detected fission fragment from the studied $^{238}$U nucleus is opposite to and coincides with the direction of the beam. The orientation was changed by rotating the cylindrical chamber with MWPCs by 180° about the axis that passes through its center and is perpendicular to the direction of the neutron beam. This rotation also allowed us to minimize effects caused by the attenuation of the neutron flux in the targets and MWPCs.

Fission fragments of the studied and reference nuclei in relative measurements are detected by the same MWPCs. Consequently, when processing data, it is necessary to identify a fissioning nucleus whose fragment is detected. Since a fission fragment of the studied and reference nuclei moves from the first to the second MWPC and from the second to the first MWPC, respectively, this identification can be ensured by measuring the time of flight of the fission fragment from the cathode C2 of MWPC2 to the cathode C1 of MWPC1. Figure 2 shows the time-of-flight spectra of fission fragments for certain scattering angles of fission fragments with respect to the normal to the plane of electrodes of the MWPCs obtained in one measuring run. Two separate groups of events corresponding to $^{238}$U($n$, $f$) and $^{235}$U($n$, $f$) fissions are clearly seen.

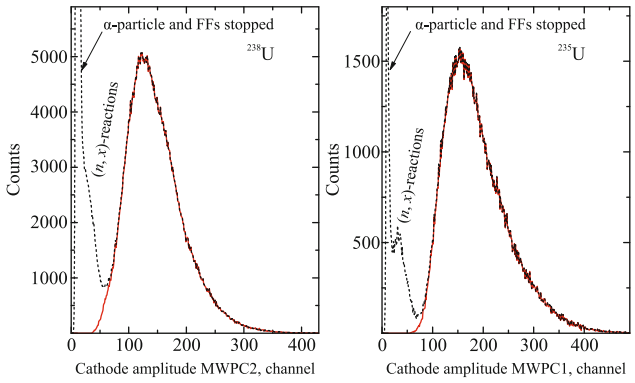


**Fig. 3.** (Color online) Amplitude spectrum of signals from the cathode of the multiwire proportional counter nearest to the (left panel) $^{238}$U and (right panel) $^{235}$U targets. The red solid and black dashed lines are the spectra after and before the selection of desired fission events, respectively.

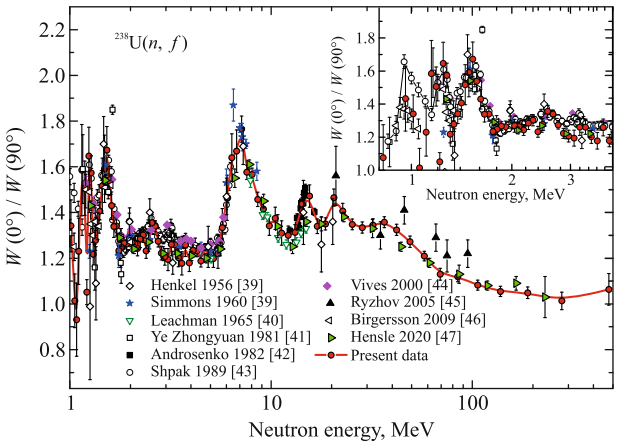


**Fig. 4.** (Color online) Anisotropy of the angular distribution of fission fragments from $^{238}$U nuclei in comparison with experimental data from [38–47]. Statistical errors are indicated. The solid line is a guide for the eye.

The further selection of fission events was similar to that described in detail in [34, 35]. For example, amplitude spectra from the cathode of the MWPCs obtained before and after the separation of "desired" fission events are shown in Fig. 3. It is remarkable that desired fission events are almost completely separated from neutron-induced background reactions in the substrate of the target and in other materials of the detector.

The efficiency of the detection of fission fragments by the array of two position-sensitive MWPCs was calculated by the Monte Carlo method taking into account the geometry of the MWPCs, as well as the profile of the neutron beam, the dimensions of the active spot on the target separated by the screen, and the spatial resolution of the MWPCs, which are associated with the measurement procedure. The efficiency of detection of fission fragments was ~45%, and the maximum angle of detection of fission fragments with respect to the normal to the plane of the electrodes of the MWPCs was 71°. The efficiencies of detection of fission fragments from the reference $^{235}$U and studied $^{238}$U nuclei were the same because the geometry and conditions of measurements for them were identical.

We also note that the distance between two MWPCs in this geometry was 20 mm, which is much larger than 3 mm in [32–37]. As a result, we avoided the distortion of angular distributions of fission fragments caused by the mutual effects of signals (the so-called "crosstalk" effect) from the anodes of two MWPCs, and additional corrections introduced in previous works were unnecessary.

Figure 4 presents the anisotropy $W(0°)/W(90°)$ of the angular distribution of fission fragments from $^{238}$U nuclei at neutron energies of 0.8–500 MeV according to this work and our previous measurements [33]. Fission events in [33] were separated using only amplitude spectra from the cathodes of MWPCs under the assumption that the efficiency of the detection of fission fragments is independent on the detection angle. This procedure can lead to the distortion of previous dependences. For this reason, we reprocessed the data obtained in [33] as in our later works [34–37]. It was found that the difference between the data obtained in [33] and the results of the joint processing of data in this work is within the measurement errors. For this reason, only results of the joint processing of data are shown in Fig. 4, where experimental data obtained by other authors [38–47] taken from the EXFOR [7] are also given. The inset of Fig. 4 presents the anisotropy of the angular distribution of fission fragments at neutron energies below 4.0 MeV. Fission fragments were detected in the cited works using proportional gas counters [39], "catching" foils [40], "track" detectors [41–43], a fission ionization chamber with a grid [38, 44–46], and a time projection chamber [47].

General agreement between data on the anisotropy of the angular distribution of fission fragments obtained in this work and data obtained by other authors at neutron energies below 20 MeV can confirm the accuracy and reliability of our method of measurement and data processing because methods used by various authors differ both in type of detectors and in properties of neutron sources. Our data for neutron energies above 20 MeV are in agreement within the experimental errors with measurements at the Los Alamos Neutron Science Center [47], whereas data reported in [45] demonstrate a higher anisotropy of angular distributions of fission fragments.

Our results for the ratio $R(E) = \sigma_f^{U8}/\sigma_f^{U5}$ of the fission cross sections of $^{238}$U and $^{235}$U nuclei are shown in Fig. 5 in comparison with data obtained in [22–25] and taken from the EXFOR database.

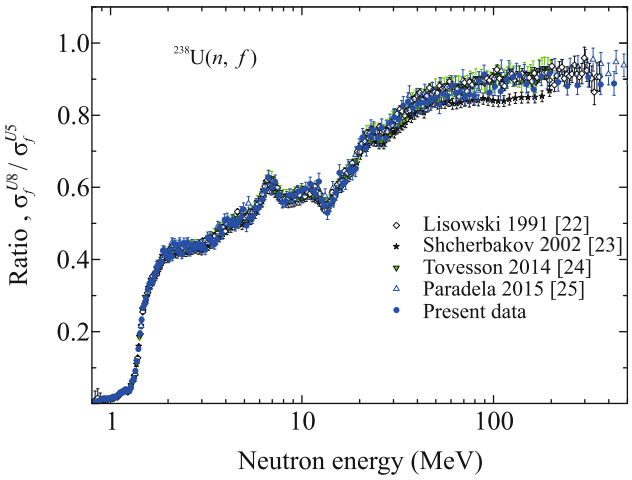


**Fig. 5.** (Color online) Ratio of the fission cross sections of $^{238}$U and $^{235}$U nuclei according to our measurements and other experimental data taken from the EXFOR database.

When determining the ratio $R$, we took into account the correction to both the anisotropy of angular distributions of fission fragments and the limited solid angle of their detection. This correction was about 2% on average and was determined using the anisotropy of angular distributions of fission fragments from $^{238}$U and $^{235}$U nuclei obtained in the joint analysis of our previous measurements [33] and data reported in this work. The correction to the isotope composition of the targets was also taken into account. It is less than 0.1% at neutron energies above 1 MeV, increases with decreasing neutron energy, and reaches a maximum of 8% at a neutron energy of 0.3 MeV. The relative errors of the ratio of fission cross sections measured in this work are summarized in Table 1. The average statistical accuracy reached in this work at energies above 1.4 MeV is 2.4%. The total average systematic error of measurements is 1.9% and is determined to a great extent by an uncertainty of 1.2% in the correction to the anisotropy of the angular distribution of fission fragments and an uncertainty of 1.5% in the normalization factor.

**Table 1.** Relative errors of measurements of the ratio $R$ of the fission cross sections of $^{238}$U and $^{235}$U nuclei

| | |
|---|---|
| Statistical accuracy | 60–2.4% (0.3–1.4 MeV)<br>2.4% (above 1.4 MeV) |
| Attenuation of the neutron flux | <0.3% |
| Anisotropy | 10% (below 0.8 MeV)<br>3% (0.8–1.2 MeV)<br>1.2% (above 1.2 MeV) |
| Purity of targets | 2% (below 0.8 MeV)<br>0.2% (0.8–2.0 MeV)<br>~$10^{-4}$% (above 2 MeV) |
| Efficiency of multiwire proportional counters (geometrical uncertainty) | 0.3% |
| Normalization factor $N_{U8}/N_{U5}$ | 1.5% |
| Total error | 3.1% |
| Uncertainty of the $^{235}$U standard | |
| $\sigma_f(^{235}\mathrm{U})$ | 1.3–1.5% (below 20 MeV)<br>1.5–4.8% (20–200 MeV)<br>5–7% (above 200 MeV) |

We obtained the $^{238}$U($n$, $f$) fission cross section as the product of the measured ratio $R$ and the $\sigma_f(^{235}\mathrm{U})$ standard, i.e., the $^{235}$U($n$, $f$) fission cross section [5, 6]. Figure 6 shows the $^{238}$U($n$, $f$) fission cross section obtained in this work in comparison with data from some works cited above and with the estimate from the ENDF/B-VIII.0 library [48]. We note that this estimate in the neutron energy range of 2–30 MeV almost coincides with the recommended $^{238}$U($n$, $f$) fission cross section [5, 6]. The $^{238}$U($n$, $f$) fission cross section in all works cited in Fig. 6 was determined as the product of the measured ratio $R$ and the $\sigma_f(^{235}\mathrm{U})$ standard, except for [27], where the neutron flux had a high uncertainty of ~10% because of the geometry of the experiment and the measured ratio of the fission cross sections of $^{238}$U and $^{235}$U nuclei was normalized to the ratio of the fission cross sections of $^{238}$U and $^{235}$U nuclei at a neutron energy of 14.5 MeV from the ENDF/B-VIII.β5 evaluated nuclear data library. For this reason, for convenient comparison, these data were renormalized to the corresponding value from the ENDF/B-VIII.0 library with the normalization error taken equal to an error of 1.8% in the ratio of the recommended fission cross sections of $^{238}$U and $^{235}$U nuclei at a neutron energy of 14.5 MeV.

Only those data from [25] are shown in Fig. 6 that were obtained, as in this work, with position-sensitive detectors, which were placed perpendicularly to the neutron beam inducing fission. Similarly, only those data from [26] are shown in Fig. 6 that were obtained with a multisection ionization chamber because a minimum neutron energy of ~0.3 MeV was reached in this case.

The comparison of the results presented in Fig. 6 shows general agreement within the total error (the error of the fission cross section of $^{235}$U nuclei taken as the standard is not included) between data of this work and data obtained by other authors and the estimate from the ENDF/B-VIII.0 library. Nevertheless, some differences remain, as seen in Fig. 7, which presents the ratio of the data shown in Fig. 6 to the estimate from the ENDF/B-VIII.0 library. The measurements in all works cited in Fig. 7 were performed with neutron beams with a continuous spectrum using the

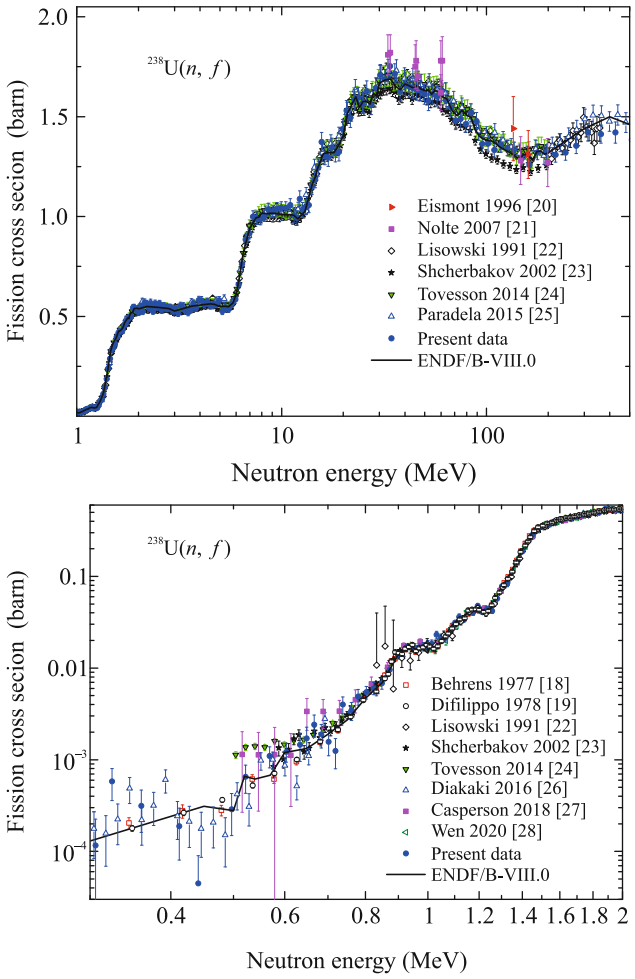


**Fig. 6.** (Color online) Cross sections for the neutron-induced fission of $^{238}$U nuclei obtained in this work and in [18–28] with total errors. The solid line consists of the estimate from the ENDF/B-VIII.0 library below 30 MeV and the cross section recommended in [5, 6] above 30 MeV.

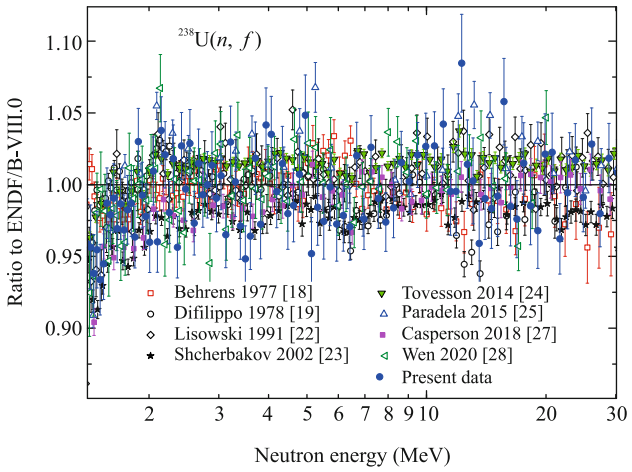


**Fig. 7.** (Color online) Ratio of the fission cross sections of $^{238}$U nuclei obtained in this work and in other time-of-flight measurements to the estimate for this cross section from the ENDF/B-VIII.0 library. Statistical errors are indicated.

time-of-flight method with respect to the fission cross section of $^{235}$U. The comparison of the presented data shows that the ratio of experimental data to the estimate from the ENDF/B-VIII.0 library is independent of the neutron energy in the range of 2–30 MeV within the statistical error of measurements. The existing average deviation does not exceed the experimental accuracy of the determination of the normalization factor related to the uncertainty in the thickness of the targets and in the detection efficiency of the detector of fission fragments and neutron flux (scaling factor). This is seen in Fig. 8, where the average deviation of data from the estimate from the ENDF/B-VIII.0 library and the error of the resulting average deviation, which was determined from the spread of experimental points with respect to this average deviation, as well as experimental errors attributed to the normalization, are presented. The dependences shown in Figs. 7 and 8 can indicate that the shape of the fission cross section of $^{238}$U nuclei from the ENDF/B-VIII.0 library quite correctly describes existing experimental data obtained with neutron beams with a continuous spectrum using the time-of-flight method. The authors of recent work [29] (data obtained in [29] have not yet been included in the EXFOR database) also noted that the shape of the measured $^{238}$U($n$, $f$) fission cross section is in agreement with the estimate from the ENDF/B-VIII.0 library, and the average deviation from this estimate at neutron energies of 0.5–200 MeV is 0.02–0.13% (at an uncertainty of ~1.6% in the normalization factor).

A more detailed comparison of the experimental data presented in Fig. 7 reveals some features. In particular, the shape of the fission cross section from the ENDF/B-VIII.0 library almost ideally describes the data from [23, 24], whereas the deviation of the data reported in [18, 19, 27] from this fission cross section depends on the neutron energy: this deviation decreases by ~2% with increasing neutron energy in [18, 19] and increases by ~2% in [27]. This indicates the absence of significant systematic errors in the experimental data presented above, which change the energy dependence of the fission cross section.

It is noteworthy that the aforementioned difference in the cited data at neutron energies above 100 MeV will disappear if the experimental fission cross sections of $^{238}$U nuclei from [22–25] are normalized to the recommended fission cross section of $^{238}$U, e.g., in the neutron energy range of 2–5 MeV, because these data will coincide within experimental errors with each other and the recommended fission cross section of $^{238}$U nuclei will coincide within its errors with all experimental data.

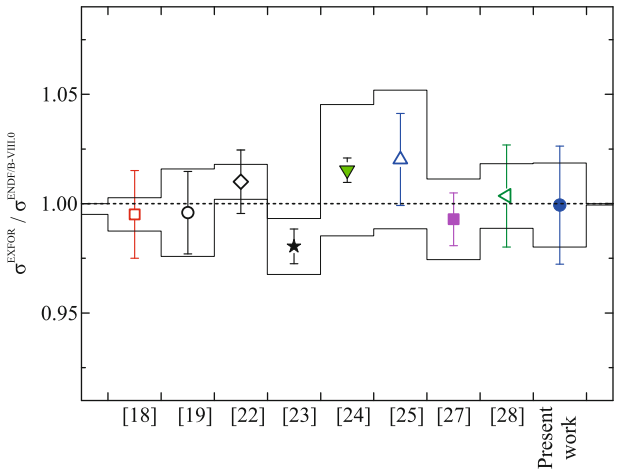


**Fig. 8.** (Color online) Standard deviation of the fission cross sections of $^{238}$U nuclei obtained in the discussed works from the estimate from the ENDF/B-VIII.0 library. The solid line indicates errors attributed to the normalization to the number of nuclei and the efficiency of detection of fission fragments and neutron flux.

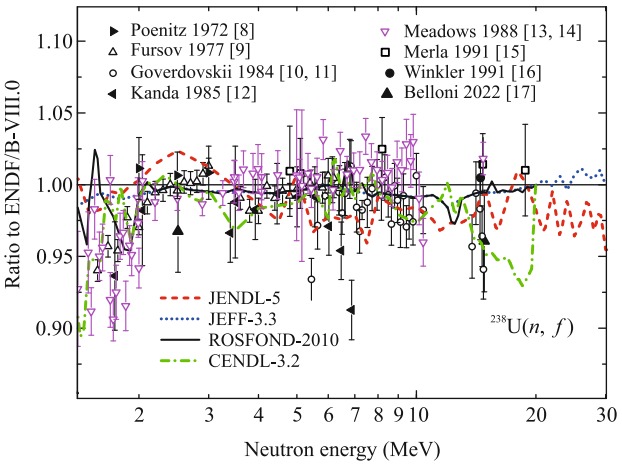


**Fig. 9.** (Color online) Ratio of the fission cross sections of $^{238}$U nuclei obtained in the discussed works to the estimate from the ENDF/B-VIII.0 library with total errors.

Figure 9 shows the ratio of accelerator experimental data obtained at certain energies using various experimental methods to the estimate for the cross section for the neutron-induced fission of $^{238}$U nuclei from the ENDF/B-VIII.0 library. It is seen that the estimate from the ENDF/B-VIII.0 library in this case is also correct at neutron energies of 2–20 MeV. Differences between different national evaluated nuclear data libraries ROSFOND-2010 [49], JEFF-3.3 [50], JENDL-5 [51], CENDL-3.2 [52], and ENDF/B-VIII.0 are also presented in Fig. 9. All estimates are in agreement with each other with an accuracy of ~2% in the indicated energy range, except for the estimate from the CENDL-3.2 library, whose deviation increases at neutron energies above 10 MeV and reaches 7% at neutron energies near 20 MeV.

To summarize, new measurements of the fission cross section of $^{238}$U nuclei have been carried out at neutron energies up to 500 MeV. The data obtained at energies up to 30 MeV are in agreement both with numerous experimental works performed with various neutron sources and with the estimate from the international ENDF/B-VIII.0 library. Our data obtained at neutron energies above 30 MeV are also in agreement with the recommended fission cross section of $^{238}$U nuclei [5, 6]. This agreement indicates that our method is reliable and can be used to obtain data on fission cross sections of nuclei and on angular distributions of fission fragments, which are necessary for the development of new nuclear technologies.

## ACKNOWLEDGMENTS

We are grateful to E.M. Ivanov and the staff of the Accelerator Department, Petersburg Nuclear Physics Institute, for their permanent friendly assistance and smooth operation of the synchrocyclotron during the experiment and to L.S. Falev for assistance in the fabrication of the experimental setup and in the execution of the experiment.

## OPEN ACCESS



## REFERENCES

1. *Technology Roadmap Update for Generation IV Nuclear Energy Systems* (OECD-NEA, Paris, 2014).
2. A. P. Glebov, Vopr. At. Nauki Tekh., Ser.: Yad.-Reakt. Konst., No. 1, 77 (2020).
3. Report IAEA-TECDOC Series No. 1766 (IAEA, Vienna, 2015).
4. Report IAEA-TECDOC Series No. 1975 (IAEA, Vienna, 2021).
5. A. D. Carlson, V. G. Pronyaev, R. Capote, et al., Nucl. Data Sheets **148**, 143 (2018).
6. B. Marcinkevicius, S. Simakov, and V. Pronyaev, IAEA Report No. INDC(NDS)-0681 (2015); https://nds.iaea.org/standards/.

7. Int. Collab. Nucl. React. Data Centres (NRDC), Nucl. Data Sheets **120**, 272 (2014); Nuclear Reaction Data Library (EXFOR). https://www-nds.iaea.org/exfor/.
8. W. P. Poenitz and R. J. Armani, J. Nucl. Energy **26**, 483 (1972).
9. B. I. Fursov, V. M. Kupriyanov, B. K. Maslennikov, and G. N. Smirenkin, Sov. At. Energy **43**, 808 (1977); EXFOR 40506002.
10. A. A. Goverdovskii, B. D. Kuz'minov, V. F. Mitrofanov, et al., Sov. At. Energy **56**, 173 (1984); EXFOR 40831003.
11. A. A. Goverdovskii, A. K. Gordyushin, B. D. Kuz'minov, A. I. Sergachev, S. M. Solov'ev, and P. S. Soloshenkov, Sov. At. Energy **56**, 176 (1984); EXFOR 40831004.
12. K. Kanda, O. Sato, K. Yoshida, H. Imaruoka, and N. Hirakawa, in *Proceedings of the 1984 Seminar on Nuclear Data, JAERI, Japan, 1985,* Ed. by T. Asami and S. Igarasi, INDC(JPN)-98/G (JAERI, Japan, 1985), p. 220; EXFOR 21963006. https://www-nds.iaea.org/publications/indc/indc-jpn-0098/.
13. J. W. Meadows, Report No. ANL/NDM-83 (Argonne Natl. Labor., 1983); https://www.ne.anl.gov/capabilities/nd/reports/ANLNDM-083.pdf. EXFOR 10237003, 10506002.
14. J. W. Meadows, Ann. Nucl. Energy **15**, 421 (1988); EXFOR 13134007.
15. K. Merla, P. Hausch, C. M. Herbach, G. Musiol, G. Pausch, U. Todt, L. V. Drapchinsky, V. A. Kalinin, and V. I. Shpakov, in *Proceedings of the International Conference on Nuclear Data for Science and Technology, Julich, Germany, May 13–17, 1991* (Springer, Germany, 1992), p. 510; EXFOR 22304003.
16. G. Winkler, V. E. Lewis, T. B. Ryves, and M. Wagner, in *Report Nuclear Data for Science and Technology, Julich, Germany, May 13–17, 1991* (Springer, Germany, 1992), p. 514; EXFOR 22565002.
17. F. Belloni, R. Eykens, J. Heyse, C. Matei, A. Moens, R. Nolte, A. J. M. Plompen, S. Richter, G. Sibbens, D. Vanleeuw, and R. Wynants, Eur. Phys. J. A **58**, 227 (2022).
18. J. W. Behrens and G. W. Carlson, Nucl. Sci. Eng. **63**, 250 (1977); EXFOR 32798002.
19. F. C. Difilippo, R. B. Perez, G. de Saussure, D. K. Olsen, and R. W. Ingle, Nucl. Sci. Eng. **68**, 43 (1978); EXFOR 10635002.
20. V. P. Eismont, A. V. Prokofiev, A. N. Smirnov, K. Elmgren, J. Blomgren, H. Condé, J. Nilsson, N. Olsson, T. Rönnqvist, and E. Tranéus, Phys. Rev. C **53**, 2911 (1996).
21. R. Nolte, M. S. Allie, F. D. Brooks, A. Buffler, V. Dangendorf, J. P. Meulders, H. Schuhmacher, F. D. Smit, and M. Weierganz, Nucl. Sci. Eng. **156**, 197 (2007); EXFOR 23078003.
22. P. W. Lisowski, A. Gavron, W. E. Parker, J. L. Ullmann, S. J. Balestrini, A. D. Carlson, O. A. Wasson, and N. W. Hill, in *Proceedings of the NENADC Specialists Meeting on Neutron Cross Section Standards for the Energy Region above 20 MeV, Uppsala, Sweden, May 21–23, 1991,* NEADC Report No. 305 (1991), p. 177; EXFOR 14016003.
23. O. Shcherbakov, A. Donets, A. Evdokimov, A. Fomichev, T. Fukahori, A. Hasegawa, A. Laptev, V. Maslov, G. Petrov, Yu. Tuboltsev, and A. Vorobiev, J. Nucl. Sci. Technol. **39**, 230 (2002); EXFOR 41455003.
24. F. Tovesson, A. Laptev, and T. S. Hill, Nucl. Sci. Eng. **178**, 57 (2014); EXFOR 14402009.
25. C. Paradela, M. Calviani, D. Tarrio, et al. (n_TOF Collab.), Phys. Rev. C **91**, 024602 (2015); EXFOR 23269003.
26. M. Diakaki, L. Audouin, E. Berthoumieux, et al. (n_TOF Collab.), EPJ Web Conf. **111**, 02002 (2016); EXFOR 23269006.
27. R. J. Casperson, D. M. Asner, J. Baker, et al. (NIFFTE Collab.), Phys. Rev. C **97**, 034618 (2018); EXFOR 14498002.
28. J. Wen, Y. Yang, Zh. Wen, et al., Ann. Nucl. Energy **140**, 107301 (2020); EXFOR 32798002.
29. Zh. Ren, Y. Yang, R. Liu, et al., Eur. Phys. J. A **59**, 5 (2023).
30. N. K. Abrosimov, G. Z. Borukhovich, A. B. Laptev, V. V. Marchenkov, G. A. Petrov, O. A. Shcherbakov, Yu. V. Tuboltsev, and V. I. Yurchenko, Nucl. Instrum. Methods Phys. Res., Sect. A **242**, 121 (1985).
31. O. A. Shcherbakov, A. S. Vorobyev, and E. M. Ivanov, Phys. Part. Nucl. **49**, 81 (2018).
32. A. M. Gagarski, A. S. Vorobyev, O. A. Shcherbakov, and L. A. Vaishnene, in *Proceedings of XXIV International Seminar on Fundamental Interactions and Neutrons, Nuclear Structure, Ultracold Neutrons, Related Topics ISINN-24, Dubna, May 24–27, 2016,* JINR Preprint E3-2017-8 (Dubna, JINR, 2017), p. 343.
33. A. S. Vorobyev, A. M. Gagarski, O. A. Shcherbakov, L. A. Vaishnene, and A. L. Barabanov, JETP Lett. **102**, 203 (2015); EXFOR 41608004.
34. A. S. Vorobyev, A. M. Gagarski, O. A. Shcherbakov, L. A. Vaishnene, and A. L. Barabanov, JETP Lett. **104**, 365 (2016).
35. A. S. Vorobyev, A. M. Gagarski, O. A. Shcherbakov, L. A. Vaishnene, and A. L. Barabanov, JETP Lett. **107**, 521 (2018).
36. A. S. Vorobyev, A. M. Gagarski, O. A. Shcherbakov, L. A. Vaishnene, and A. L. Barabanov, JETP Lett. **110**, 242 (2019).
37. A. S. Vorobyev, A. M. Gagarski, O. A. Shcherbakov, L. A. Vaishnene, and A. L. Barabanov, JETP Lett. **112**, 323 (2020).
38. R. L. Henkel and J. E. Brolley, Jr., Phys. Rev. **103**, 1292 (1956); EXFOR 13709003.
39. J. E. Simmons and R. L. Henkel, Phys. Rev. **120**, 198 (1960).
40. R. B. Leachman and L. Blumberg, Phys. Rev. B **137,** 814 (1965); EXFOR 13708006.
41. Y. Zhongyuan, L. Jingwen, Zh. Shuhua, and H. Xiuhong, Sci. China, Ser. A **25**, 502 (1982); EXFOR 30693003.
42. Kh. D. Androsenko, G. G. Korolev, and D. L. Shpak, Vopr. At. Nauki Tekh., Ser.: Yad. Konst. **46** (2), 9 (1982); IAEA Report No. INDC(CCP)-193 (IAEA, 1982), p. 9. https://www-nds.iaea.org/publications/indc/indc-ccp-0193.pdf); EXFOR 40825005.

43. D. L. Shpak, Sov. J. Nucl. Phys. **50**, 574 (1989); EXFOR 41041002.
44. F. Vives, F.-J. Hambsch, H. Bax, and S. Oberstedt, Nucl. Phys. A **662**, 63 (2000); EXFOR 22402003.
45. I. V. Ryzhov, M. S. Onegin, G. A. Tutin, J. Blomgren, N. Olsson, A. V. Prokofiev, and P.-U. Renberg, Nucl. Phys. A **760**, 19 (2005); EXFOR 22898003.
46. E. Birgersson, A. Oberstedt, S. Oberstedt, and F.-J. Hambsch, Nucl. Phys. A **817**, 1 (2009); EXFOR 23054003.
47. D. Hensle, J. T. Barker, J. S. Barrett, et al. (NIFFTE Collab.), Phys. Rev. C **102**, 014605 (2020); EXFOR 14660003.
48. D. A. Brown, M. B. Chadwick, R. Capote, et al., Nucl. Data Sheets **148**, 1 (2018).
49. S. V. Zabrodskaya, A. V. Ignatyuk, V. N. Koscheev, V. N. Manohin, M. N. Nikolaev, and V. G. Pronyaev, Vopr. At. Nauki Tekh., Ser.: Yad. Konst., Nos. 1–2, 3 (2007); https://www-nds.iaea.org/exfor/endf.htm.
50. OECD and NEA, *The Joint Evaluated Fission and Fusion File (JEFF), Vers. 3.3* (OECD-NEA, Paris, 2018); https://www.oecd-nea.org/dbdata/jeff/jeff33/.
51. O. Iwamoto, N. Iwamoto, K. Shibata, A. Ichihara, S. Kunieda, F. Minato, and S. Nakayama, EPJ Web of Conf. **239**, 09002 (2020); https://www-nds.iaea.org/exfor/endf.htm.
52. Zh. Ge, R. Xu, H. Wu, et al., EPJ Web of Conf. **239**, 09001 (2020); https://www-nds.iaea.org/exfor/endf.htm.

*Translated by R. Tyapaev*